

Phase lapses in transmission through interacting two-level quantum dots

C Karrasch¹, T Hecht², A Weichselbaum², J von Delft², Y Oreg³, and V Meden¹

¹ Institut für Theoretische Physik, Universität Göttingen, 37077 Göttingen, Germany

E-mail: meden@theorie.physik.uni-goettingen.de

² Physics Department, Arnold Sommerfeld Center for Theoretical Physics and Center for NanoScience, Ludwig-Maximilians-Universität, 80333 Munich, Germany

³ Department of Condensed Matter Physics, The Weizmann Institute of Science, Rehovot 76100, Israel

Abstract. We investigate the appearance of π lapses in the transmission phase θ of a two-level quantum dot with Coulomb interaction U . Using the numerical and functional renormalization group methods we study the entire parameter space for spin-polarized as well as spin-degenerate dots, modeled by spinless or spinful electrons, respectively. We investigate the effect of finite temperatures T . For small T and sufficiently small single-particle spacings δ of the dot levels we find π phase lapses between two transmission peaks in an overwhelming part of the parameter space of the level-lead couplings. For large δ the appearance or not of a phase lapse between resonances depends on the relative sign of the level-lead couplings in analogy to the $U = 0$ case. We show that this generic scenario is the same for spin-polarized and spin-degenerate dots. We emphasize that in contrast to dots with more levels, for a two-level dot with small δ and generic dot-lead couplings (that is up to cases with special symmetry) the “universal” phase lapse behavior is already established at $U = 0$. The most important effect of the Coulomb interaction is to increase the separation of the transmission resonances. The relation of the appearance of phase lapses to the inversion of the population of the dot levels is discussed. For the spin-polarized case and low temperatures we compare our results to recent mean-field studies. For small δ correlations are found to strongly alter the mean-field picture.

PACS numbers: 73.23.-b, 73.63.Kv, 73.23.Hk

1. Introduction

The local Coulomb interaction $U > 0$ of electrons occupying quantum dots leads to a variety of effects. Many of them can conveniently be studied in transport through the dot within the linear regime. Theoretically as well as experimentally well-investigated examples are the Coulomb blockade (CB) peaks of the transmission (conductance) [1] as well as the plateaus of width U of the transmission (conductance) induced by the Kondo effect [2]. Additional features of interacting multi-level dots that have recently attracted considerable theoretical attention are the population inversions of the dot levels [3, 4, 5, 6], the phase lapses of the transmission phase θ or, equivalently, the zeros of the transmission amplitude t (transmission zeros) [3, 7, 8, 9, 10, 11] and additional correlation-induced resonances of $|t|$ [12]. They appear in certain parts of the parameter space when the level occupancies and the transmission amplitude are investigated as functions of the level positions, which can be tuned via a nearby plunger gate voltage. Such effects were hitherto mostly studied in a minimal model involving only two levels. A very important step towards a unified understanding of population inversions, phase lapses and correlation-induced resonances in spin-polarized two-level dots was recently taken by a multi-stage mapping of the problem on a generalized Kondo model and a subsequent renormalization group and Bethe ansatz analysis of the effective Hamiltonian [13].

Theoretical studies of phase lapses (transmission zeros) are of primary interest in connection with a series of linear response transmission measurements by the Weizman group [14, 15, 16] on Aharonov-Bohm rings containing a quantum dot in one arm. Under suitable conditions both the phase θ and magnitude $|t|$ of the transmission amplitude $t = |t|e^{i\theta}$ of the dot can be extracted from the Aharonov-Bohm oscillations of the current through the ring [17]. When this is done as function of a plunger gate voltage V_g that linearly shifts the dot's single-particle energy levels downward, $\varepsilon_j = \varepsilon_j^0 - V_g$ ($j = 1, 2, \dots$ is a level index), a series of well-separated CB peaks of rather similar width and height was observed in $|t(V_g)|$, across which $\theta(V_g)$ continuously increased by π , as expected for Breit-Wigner-like resonances. In each CB valley between any two successive peaks, θ always jumped sharply downward by π . This phase lapse behavior was found to be “universal”, occurring in a large succession of valleys for every *many*-electron dot studied in Refs. [14, 15, 16]. This universality is puzzling, since naively the behavior of $\theta(V_g)$ is expected to be “mesoscopic”, i.e. to show a phase lapse in some CB valleys and none in others, depending on the dot's shape, the parity of its orbital wavefunctions, etc. Only recently [16], also the *few*-electron regime was probed experimentally: as V_g was increased to successively fill up the dot with electrons, starting from electron number $N_e = 0$, $\theta(V_g)$ was observed to behave mesoscopically in the *few*-electron regime, whereas the above-mentioned universal phase lapse behavior emerged only in the *many*-electron regime ($N_e \gtrsim 15$).

It was suggested in Ref. [16] that a generic difference between the few- and many-electron dots may be that for the latter, transport might simultaneously occur through

several partially filled single-particle levels in parallel. A possible reason could be that the mean (non-interacting) level spacing δ of the topmost filled levels decreases as the number of electrons increases, while the charging energy U still implies well separated transmission resonances [18]. This scenario forms the basis of a recent systematic study by us of the interplay of level spacing, level width and charging energy on the phase lapses for up to four interacting levels and spin-polarized electrons [19]. We showed that the universal phase lapse and transmission zero behavior appearing at small δ can be understood as resulting from a Fano-type interference effect [20] involving transport through two or more effective dot levels, whose position and width have been renormalized by the Coulomb interaction and coupling to the leads. The importance of several overlapping levels for phase lapses had earlier been pointed out by Silvestrov and Imry in a rather specific model of a single wide and several narrow levels with strong interaction [3].

Here we supplement our earlier study [19] by discussing the relation between phase lapses and population inversions and by investigating the role of finite temperatures $T > 0$ as well as spin, focusing on $N = 2$ levels. When spin is included, the Kondo effect plays a role for an odd average occupation of the dot, but the phase lapse scenario is unaffected by this. Experimentally the behavior of the phase in the presence of the Kondo effect was investigated in Refs. [21] and [22]. As in Ref. [19] we are concerned with the *generic* behavior and thus investigate the entire parameter space, going beyond subspaces of higher symmetry [such as left-right (l-r) or 1-2 symmetry of the coupling between the left and right leads and the two levels]. For low temperatures and sufficiently small single-particle spacings δ of the dot levels, we find π phase lapses between two transmission peaks in an overwhelmingly large part of the parameter space of the level-lead couplings. We point out that the two level case is special compared to models with $N > 2$, as for generic level-lead couplings a transmission zero and phase lapse occurs between the two transmission peaks *even at* $U=0$. The effect of the interaction is merely to increase the separation of the transmission peaks. For large δ the appearance or not of phase lapses between transmission peaks depends on the relative sign of the level-lead couplings in analogy to the noninteracting case [9].

For spin-polarized dots we in addition compare our $T = 0$ results with the ones of recent mean-field studies [10, 11]. In these works level-lead couplings beyond the subspaces with increased symmetry were studied, and a remarkably more complex behavior was found once the symmetries were broken. The importance of considering such generic parameter sets was independently pointed out in Ref. [12]. We here elucidate how the phase lapse behavior is affected by quantum fluctuations, which are expected to be strong in low-dimensional systems. We find that upon including quantum fluctuations, the part of parameter space exhibiting universal π phase lapses between well separated CB peaks becomes larger than suggested by the mean-field study. In particular, we do not recover certain peculiar features of the mean-field results of Refs. [10] and [11], namely the occurrence, in certain regimes of parameter space, of a phase lapse of less than π (instead of precisely π), accompanied by the disappearance of the

corresponding transmission zero [10, 6]. These features thus turn out to be artifacts of the mean-field approximation, which misses the rather simple scenario for the phase lapse behavior of a two-level dot at small δ : for generic level-lead couplings a phase lapse and transmission zero between two transmission peaks is already present at $U = 0$; increasing the Coulomb interaction the peaks become well separated while the phase lapse and transmission zero remain in the valley between them.

In the model of a single wide and several narrow levels [3] a relation between phase lapses and population inversions was discussed. Therefore, in phase lapse studies quite often also the level occupancies n_j , $j = 1, 2$, are investigated. We emphasize that the generic appearance of a phase lapse and transmission zero even at $U = 0$ renders the two-level model unsuitable for establishing a general relation between phase lapses and population inversions, as the latter only appear at sufficiently large U . Furthermore, we show that discontinuities of the n_j as a function of V_g are an artifact of the mean-field solution (see Refs. [10] and [6]). Within our approaches discontinuities are only found for l-r symmetric level-lead couplings with a relative plus sign of the underlying hopping matrix elements and degenerate levels, a case which was earlier identified as being nongeneric [12, 13], because the transmission shows only a single peak.

This paper is organized as follows. In Sec. 2 we introduce our model for the spin-polarized and spin-degenerate two-level dot. We discuss the relation between the measured magnetic flux dependence of the interferometer's linear conductance and the magnitude and phase of the dot's transmission amplitude. The latter can be computed from the one-particle Green function of the dot. We present a brief account of our techniques to obtain the latter, the numerical (NRG) [23] and functional renormalization group (fRG) methods. For an introduction to the use of the fRG to quantum dots see Refs. [24] and [25]. In contrast to the implementation of the NRG used in Ref. [19], where we were restricted to l-r symmetric dots at $T = 0$, we have now adopted the full density matrix (FDM) NRG method of [26], which enables us to investigate dots with arbitrary level-lead state overlap matrix elements t_j^l (with $l = L, R$) as well as to study finite temperatures. In Secs. 3-5 we present our results of the V_g dependence of $|t|$ and θ . First we briefly discuss the noninteracting two-level dot with generic level-lead couplings and point out that the phase lapse scenario differs from the one for more than two levels. We then investigate interacting, spin-polarized dots, study the relation between phase lapses and population inversions and compare to the mean-field results for the phase lapses. The issue of continuous versus discontinuous V_g dependence of the level occupancies n_1 and n_2 is commented on. Next we study the role of finite temperatures. Finally, we consider spin-degenerate levels at small T which implies the appearance of Kondo physics at odd average dot filling. Using NRG and fRG we show that the spin does not alter the universal phase lapse scenario. Our findings are summarized in Sec. 6.

2. The model and methods

In this section we introduce our model for the two-level dot. We argue that it is the energy dependent (effective) transmission amplitude $\tilde{t}(\omega)$ which one has to compute if one is interested in comparing to the measurements of Refs. [14, 15, 16] of the magnitude of the transmission amplitude and its phase. The amplitude $\tilde{t}(\omega)$ can be determined from the matrix elements of the dot's interacting one-particle Green function. We furthermore discuss aspects of the NRG and the fRG specific to our problem.

2.1. Two-level setup and transmission amplitude

Our Hamiltonian consists of three parts

$$H = H_{\text{lead}} + H_{\text{dot}} + H_{\text{lead-dot}}. \quad (1)$$

The two semi-infinite leads are modeled as noninteracting one-dimensional tight-binding chains and for simplicity are assumed to be equal

$$H_{\text{lead}} = -\tau \sum_{l=L,R} \sum_{\sigma} \sum_{m=0}^{\infty} (c_{m,\sigma,l}^{\dagger} c_{m+1,\sigma,l} + \text{H.c.}). \quad (2)$$

The hopping strength in the leads is τ . We use standard second quantized notation with $l = L, R$ indicating the left and right leads, where the quantum numbers m and σ label Wannier states and spin, respectively. The dot is described by

$$H_{\text{dot}} = \sum_{\sigma} \sum_{j=1,2} \varepsilon_j d_{j,\sigma}^{\dagger} d_{j,\sigma} + \frac{1}{2} U \sum_{\sigma,\sigma'} \sum_{j,j'} \left(d_{j,\sigma}^{\dagger} d_{j,\sigma} - \frac{1}{2} \right) \left(d_{j',\sigma'}^{\dagger} d_{j',\sigma'} - \frac{1}{2} \right), \quad (3)$$

where the term with $j = j'$ and $\sigma = \sigma'$ is excluded from the sum in the interacting part. We define $\varepsilon_{1/2} = \mp \delta/2 - V_g$. In experimental systems the inter- and intra-level Coulomb repulsion can be expected to be comparable in size and to avoid a proliferation of parameters we assumed them to be equal. This assumption is not essential; by relaxing it we have checked that our results are robust against inter-level variations of the interaction strengths. Finally, the coupling between dot and lead states is given by

$$H_{\text{lead-dot}} = - \sum_{l=L,R} \sum_{\sigma} \sum_{j=1,2} (t_j^l c_{0,\sigma,l}^{\dagger} d_{j,\sigma} + \text{H.c.}) \quad (4)$$

with real overlap matrix elements t_j^l . For later purposes we define $s = \text{sign}(t_1^L t_1^R t_2^L t_2^R)$ and $\gamma = \{\Gamma_1^L, \Gamma_1^R, \Gamma_2^L, \Gamma_2^R\}/\Gamma$.

For simplicity, part of our studies will be performed on a model of spinless electrons, for which the spin index will be dropped. The resulting model may be regarded as a spin-polarized version of the spinful model obtained if the latter is put in a very large magnetic field.

The experimental two-path interferometer is characterized by wide base regions and very narrow point contacts towards the emitter and collector. Electrons can thus only pass once through either the upper or lower arm (one of them containing the dot) before reaching the collector. It is furthermore reasonable to assume that the

voltage drops at the point contacts and the dot remains in equilibrium [17]. Under these conditions the magnetic flux ϕ dependent part of the conductance of the Aharonov-Bohm interferometer G_{AB} is given by [17, 27, 16]

$$G_{AB} \propto - \int_{-\infty}^{\infty} d\omega f'(\omega) |t_{\text{dot}}(\omega)| |t_{\text{ref}}| \cos [2\pi\phi/\phi_0 + \theta_{\text{ref}} + \theta_{\text{dot}}(\omega)] \quad (5)$$

with the flux quantum ϕ_0 , the derivative f' of the Fermi function as well as the transmission amplitudes $t_{\text{dot}} = |t_{\text{dot}}|e^{i\theta_{\text{dot}}}$ of the arm containing the dot and $t_{\text{ref}} = |t_{\text{ref}}|e^{i\theta_{\text{ref}}}$ of the reference arm. The transmission t_{dot} is the product of the transmission \tilde{t} through the dot and the transmission t_{rest} through the rest of the interferometer arm containing the dot. It is reasonable to assume that t_{rest} as well as t_{ref} are only weakly energy and gate voltage dependent and thus the V_g -dependence of the Aharonov-Bohm oscillations of the measured linear conductance of the interferometer is dominated by the V_g dependence of the magnitude and phase of the transmission amplitude through the dot. As usual [9], we compute the energy-averaged transmission phase θ and magnitude $|t|$ of the dot for a fixed spin direction as the phase and absolute value of

$$t(V_g) = - \int_{-\infty}^{\infty} d\omega f'(\omega) \tilde{t}(\omega) , \quad (6)$$

where the frequency integral represents an energy average, weighted by the derivative of the Fermi function, as appropriate for a finite electron temperature in the leads. In the limit $T \rightarrow 0$, $-f'$ reduces to a δ -function and $t(V_g)$ is equal to $\tilde{t}(\mu)$. We here take the chemical potential $\mu = 0$.

Using scattering theory $\tilde{t}(\omega)$ (for fixed spin direction) can be related to the spin-independent matrix elements (in the $j = 1, 2$ indices of the Wannier states) of the dot's one-particle retarded Green function \mathcal{G}

$$\begin{aligned} \tilde{t}(\omega) = 2 \left(\sqrt{\Gamma_1^L \Gamma_1^R} \mathcal{G}_{1,1}(\omega + i0) + \sqrt{\Gamma_2^L \Gamma_1^R} \mathcal{G}_{1,2}(\omega + i0) \right. \\ \left. + s \sqrt{\Gamma_1^L \Gamma_2^R} \mathcal{G}_{2,1}(\omega + i0) + s \sqrt{\Gamma_2^L \Gamma_2^R} \mathcal{G}_{2,2}(\omega + i0) \right) , \end{aligned} \quad (7)$$

with (after taking the wide band limit; see below)

$$\Gamma_j^l = \pi |t_j^l|^2 \rho_{\text{lead}}(0) \geq 0 , \quad (8)$$

where $\rho_{\text{lead}}(\omega)$ denotes the local density of states at the end of each semi-infinite lead. Without loss of generality we have assumed that $t_1^l \geq 0$, $t_2^l \geq 0$ and $t_2^R = s|t_2^R|$. The spin-independent dot occupancies n_j (per spin direction), that we will also investigate, follow from the Green function $\mathcal{G}_{j,j}$ by integrating over frequency (or can be computed directly when using NRG). For l-r symmetry of the level-lead couplings and at temperature $T = 0$, $\tilde{t}(0)$ can also be expressed in terms of the spin independent occupancies [19]

$$\tilde{t}(0) = \sin([n_e - n_o]\pi) e^{i(n_e + n_o)/\pi} , \quad (9)$$

where $n_e = n_1 + n_2$, $n_o = 0$ for $s = +$ and $n_e = n_1$, $n_o = n_2$ for $s = -$, respectively. Here we will compute \mathcal{G} in two ways, using both a truncated, that is approximate, fRG scheme, and a numerically exact method, the NRG.

2.2. The fRG approach

The truncated fRG is an approximation scheme to obtain the self-energy Σ (and thus the one-particle Green function) and higher order vertex functions for many-body problems [28, 29, 30]. As a first step in the application of this approach to quantum dots one integrates out the noninteracting leads within the functional integral representation of our many-body problem [31]. The leads provide a frequency dependent one-particle potential on the dot levels. On the imaginary frequency axis it is given by

$$V_{j,\sigma;j',\sigma'}^{\text{lead}}(i\omega) = \sum_l t_j^l t_{j'}^l g_{\text{lead}}(i\omega) \delta_{\sigma,\sigma'} , \quad (10)$$

where $g_{\text{lead}}(i\omega)$ denotes the spin-independent Green function of the isolated semi-infinite leads taken at the last lattice site

$$g_{\text{lead}}(i\omega) = \frac{i\omega + \mu}{2 \tau^2} \left(1 - \sqrt{1 - \frac{4 \tau^2}{(i\omega + \mu)^2}} \right) . \quad (11)$$

As we are not interested in band effects we take the wide band limit. The potential then reduces to

$$V_{j,\sigma;j',\sigma'}^{\text{lead}}(i\omega) = -i \sum_l \sqrt{\Gamma_j^l \Gamma_{j'}^l} \text{sign}(\omega) \delta_{\sigma,\sigma'} . \quad (12)$$

After this step, instead of dealing with an infinite system we only have to consider the dot of two interacting levels.

In the computation of the interacting one-particle Green function projected onto the dot system the sum of the dot Hamiltonian with $U = 0$ and $V_{j,\sigma;j',\sigma'}^{\text{lead}}(i\omega)$ can be interpreted as a frequency dependent “single-particle Hamiltonian” and in the following will be denoted by $h_0(i\omega)$. For the spin-polarized case it is a 2×2 matrix in the quantum number $j = 1, 2$. Including spin, because of the additional quantum number $\sigma = \uparrow, \downarrow$, $h_0(i\omega)$ is a 4×4 matrix which is block-diagonal in σ (spin conservation). As we are here not interested in the role of a magnetic field lifting the spin-degeneracy of each level the $\sigma = \uparrow$ and $\sigma = \downarrow$ blocks are equivalent. The resolvent $\mathcal{G}_0(z) = [z - h_0(z)]^{-1}$ obtained from $h_0(z)$ is equivalent to the noninteracting propagator of our two-level many-body problem projected on the dot levels. In the generating functional of the one-particle irreducible vertex functions we replace $\mathcal{G}_0(i\omega)$ by

$$\mathcal{G}_0^\Lambda(i\omega) = \Theta(|\omega| - \Lambda) \mathcal{G}_0(i\omega) = \Theta(|\omega| - \Lambda) [i\omega - h_0(i\omega)]^{-1} \quad (13)$$

with Λ being an infrared cutoff running from ∞ down to 0. Taking the derivative with respect to Λ one can derive an exact, infinite hierarchy of coupled differential equations for vertex functions, such as the self-energy and the one-particle irreducible two-particle interaction. In particular, the flow of the self-energy Σ^Λ (one-particle vertex) is determined by Σ^Λ and the two-particle vertex γ^Λ , while the flow of γ^Λ is determined by Σ^Λ , γ^Λ , and the flowing three-particle vertex. The latter could be computed from a flow equation involving the four-particle vertex, and so on. At the end of the fRG flow $\Sigma^{\Lambda=0}$ is the self-energy Σ of the original, cutoff-free problem we are interested in [28, 29] from which the Green function \mathcal{G} can be computed using the Dyson

equation. A detailed derivation of the fRG flow equations for a general quantum many-body problem that only requires a basic knowledge of the functional integral approach to many-particle physics [31] and the application of the method for a simple toy problem is presented in Ref. [30]. For an overview of the application to quantum dots see Refs. [24] and [25].

We here truncate the infinite hierarchy of flow equations by only keeping the self-energy and the frequency-independent part of the two-particle vertex. Higher order terms can be neglected if the bare two-particle interaction is not too large. By comparison to NRG data this approximation scheme was earlier shown to provide excellent results for a variety of dot systems [12, 24, 19]. For further comparison see Fig. 7 below. The present scheme leads to a frequency-independent self-energy (see below). As finite frequency effects (inelastic processes) become important at temperatures $T > 0$, but these are not accurately treated by the level of approximation used here, in the present paper we shall show fRG results only for $T = 0$. The truncation leads to the coupled differential flow equations

$$\frac{\partial}{\partial \Lambda} \Sigma_{k',k}^{\Lambda} = -\frac{1}{2\pi} \sum_{\omega=\pm\Lambda} \sum_{l,l'} e^{i\omega 0^+} \mathcal{G}_{l,l'}^{\Lambda}(i\omega) \gamma_{k',l';k,l}^{\Lambda} \quad (14)$$

and

$$\begin{aligned} \frac{\partial}{\partial \Lambda} \gamma_{k',l';k,l}^{\Lambda} = & \frac{1}{2\pi} \sum_{\omega=\pm\Lambda} \sum_{m,m'} \sum_{n,n'} \left\{ \frac{1}{2} \mathcal{G}_{m,m'}^{\Lambda}(i\omega) \mathcal{G}_{n,n'}^{\Lambda}(-i\omega) \gamma_{k',l';m,n}^{\Lambda} \gamma_{m',n';k,l}^{\Lambda} \right. \\ & \left. + \mathcal{G}_{m,m'}^{\Lambda}(i\omega) \mathcal{G}_{n,n'}^{\Lambda}(i\omega) \left[-\gamma_{k',n';k,l}^{\Lambda} \gamma_{m',l';n,l}^{\Lambda} + \gamma_{l',n';k,m}^{\Lambda} \gamma_{m',k';n,l}^{\Lambda} \right] \right\} \end{aligned} \quad (15)$$

where k, l , etc. are multi-indices representing the quantum numbers j, σ and

$$\mathcal{G}^{\Lambda}(i\omega) = [\mathcal{G}_0^{-1}(i\omega) - \Sigma^{\Lambda}]^{-1}. \quad (16)$$

In the model with spin-degenerate levels each index k, l etc. can take four different values $j = 1, 2$ and $\sigma = \uparrow, \downarrow$ which gives 16 equations for Σ^{Λ} and 256 for the two-particle vertex. For a spin-polarized two-level dot the multi-indices take two values and one obtains 4 equations for Σ^{Λ} and 16 for the two-particle vertex. The number of independent equations can be significantly reduced (see below) taking into account the antisymmetry of the two-particle vertex and the spin symmetry (for spin-degenerate levels) both being preserved by Eqs. (14) and (15). The initial conditions at $\Lambda = \Lambda_0 \rightarrow \infty$ are given by $\Sigma_{1,1'}^{\Lambda_0} = 0$ while $\gamma_{1',2';1,2}^{\Lambda_0}$ is given by the bare antisymmetrized two-body interaction. In the spin-polarized case the only nonzero components of the two-particle vertex at $\Lambda = \Lambda_0 \rightarrow \infty$ are

$$\gamma_{1,2;1,2}^{\Lambda_0} = \gamma_{2,1;2,1}^{\Lambda_0} = U \quad \text{and} \quad \gamma_{1,2;2,1}^{\Lambda_0} = \gamma_{2,1;1,2}^{\Lambda_0} = -U. \quad (17)$$

In the model including spin the initial conditions take the form

$$\begin{aligned} \gamma_{1\uparrow,1\downarrow;1\uparrow,1\downarrow}^{\Lambda_0} = U, \quad \gamma_{1\uparrow,2\uparrow;1\uparrow,2\uparrow}^{\Lambda_0} = U, \quad \gamma_{1\uparrow,2\downarrow;1\uparrow,2\downarrow}^{\Lambda_0} = U \\ \gamma_{2\uparrow,2\downarrow;2\uparrow,2\downarrow}^{\Lambda_0} = U, \quad \gamma_{1\downarrow,2\downarrow;1\downarrow,2\downarrow}^{\Lambda_0} = U, \quad \gamma_{1\downarrow,2\uparrow;1\downarrow,2\uparrow}^{\Lambda_0} = U. \end{aligned} \quad (18)$$

All other components which do not arise out of these by permutations ($\gamma_{1,2;1',2'}^{\Lambda_0} = \gamma_{1',2';1,2}^{\Lambda_0}$ and $\gamma_{1,2;1',2'}^{\Lambda_0} = -\gamma_{1,2;2',1'}^{\Lambda_0}$) are zero. The self-energy matrix and thus the one-particle

Green function is completely independent of the spin direction and in the following we suppress the spin indices.

As already mentioned the present approximation leads to a frequency-independent self-energy. This allows for a simple single-particle interpretation of its matrix elements. The sum of the $\Sigma_{j,j}^\Lambda$ and the bare level position correspond to the flowing effective level positions, $\varepsilon_j^\Lambda = \varepsilon_j + \Sigma_{j,j}^\Lambda$, while $t^\Lambda = -\Sigma_{1,2}^\Lambda = -\Sigma_{2,1}^\Lambda$ is a hopping between the levels 1 and 2 generated in the fRG flow. The fRG formalism then reduces to a set of coupled differential flow equations for ε_j^Λ , t^Λ and a few (one in the spin-polarized case and seven for spin-degenerate levels) independent components of the two-particle vertex. These flow equations can easily be integrated numerically using standard routines. It is important to note that although we start out with intra- and inter-level Coulomb interactions of equal strengths they generically become different during the fRG flow (because of the different Γ_j^l). Furthermore, additional interaction terms which are initially zero will be generated in the flow. The set of equations significantly simplifies if the flow of the vertex is neglected while the results remain qualitatively the same. Within this additional approximation and for a spin-polarized dot the flow equations for ε_j^Λ and t^Λ are explicitly given in Ref. [12]. In certain limiting cases it is even possible to analytically solve the differential equations [12, 24]. However, in the present work, the flow of the vertex is retained which clearly improves the quality of approximation [24].

At the end of the fRG flow, the full Green function takes the form $[\mathcal{G}(i\omega)]_{j,j'}^{-1} = i\omega\delta_{j,j'} - h_{j,j'}(i\omega)$ with an effective, *noninteracting* (but V_{g-} , U - and ω -dependent) “Hamiltonian”

$$h_{j,j'}(i\omega) = h_{0;j,j'}(i\omega) - \Sigma_{j,j'} . \quad (19)$$

In a last step we have to perform the analytic continuation to the real frequency axis $i\omega \rightarrow \omega + i0$. This is straightforward, as the only frequency dependence of $h(i\omega)$ is the trivial one of the lead contribution Eq. (12). Then $\tilde{t}(\omega)$ can be computed using Eq. (7).

2.3. The NRG approach

The numerical renormalization group was invented by K. G. Wilson in 1974 as a nonperturbative renormalization scheme for the Kondo model [32]. It was later extended to the fermionic [23, 33] Anderson model which describes a localized electronic state coupled to a fermionic bath. The NRG allows thermodynamic and dynamic properties of such strongly correlated systems to be calculated at zero and finite temperature [34, 35, 36, 37, 38, 26].

The key idea of NRG is to discretize the conduction band of the bath logarithmically, leading to a tight-binding chain for which the hopping matrix elements between the successive sites fall off exponentially with $\Lambda_{\text{NRG}}^{-n/2}$, where $\Lambda_{\text{NRG}} > 1$ is the discretization parameter, typically $1 < \Lambda_{\text{NRG}} < 3$, and n is the site index. This energy scale separation ensures that the problem can be solved iteratively by adding one site at a time and diagonalizing the enlarged system at each step, thereby resolving successively

smaller and smaller energy scales. Thus, by choosing the length N of the chain so large that the corresponding energy scale $\sim \Lambda_{\text{NRG}}^{-N/2}$ is smaller than all other energies in the problem, all relevant energy scales can be resolved and treated properly. Since the dimension of the Hilbert space of the chain increases exponentially with the length of the chain, a truncation scheme has to be adopted, according to which only the lowest N_{kept} eigenstates of the chain are retained at each iteration. Recently, it was shown that by also keeping track of discarded states a complete, but approximate, basis of states can be constructed [39]. This can be used to calculate spectral functions which rigorously satisfy relevant sum rules [26].

In order to obtain the transmission through the dot $\tilde{t}(\omega)$ Eq. (7) we follow [26] and [35] to compute the imaginary part of the local Green functions at temperature T , using the Lehmann representation

$$\begin{aligned} \text{Im } \mathcal{G}_{j,j'}(\omega) = & -\pi \frac{e^{-\omega_n/T}}{Z} \langle n | d_{j,\sigma} | m \rangle \langle m | d_{j',\sigma}^\dagger | n \rangle \delta(\omega - [\omega_m - \omega_n]) \\ & -\pi \frac{e^{-\omega_n/T}}{Z} \langle n | d_{j',\sigma}^\dagger | m \rangle \langle m | d_{j,\sigma} | n \rangle \delta(\omega + [\omega_m - \omega_n]), \end{aligned} \quad (20)$$

with $Z = \sum_n e^{-\omega_n/T}$, the many-body eigenstates $|n\rangle$ and eigenenergies ω_n . Since these are causal functions, the real part can be accessed by performing a Kramers-Kronig transformation [40].

In the next three sections we present our results. In Sec. 3 for the $U = 0$ case. In Sec. 4 we present the generic phase lapse scenario for interacting spin-polarized dots, compare to the mean-field results and investigate the role of finite temperatures. Finally, in Sec. 5 we study the spinful two-level dot.

3. Results: Noninteracting dots

The large number of parameters makes it essential to analyze the transmission for the noninteracting case before considering the effect of two-particle interactions. We focus on $T = 0$. A closed expression for $|t(V_g)|$ and $\theta(V_g)$ (for a fixed spin direction) at $U = 0$ can be obtained from Eqs. (6) and (7) by replacing $\mathcal{G}(0 + i0)$ by $\mathcal{G}_0(0 + i0)$,

$$|t(V_g)| = \frac{2 \left[\Gamma_1^L \Gamma_1^R \varepsilon_2^2 + \Gamma_2^L \Gamma_2^R \varepsilon_1^2 + 2s \sqrt{\Gamma_1^L \Gamma_1^R \Gamma_2^L \Gamma_2^R} \varepsilon_1 \varepsilon_2 \right]^{1/2}}{\left[\left(\Gamma_1^L \Gamma_2^R + \Gamma_2^L \Gamma_1^R - 2s \sqrt{\Gamma_1^L \Gamma_1^R \Gamma_2^L \Gamma_2^R} - \varepsilon_1 \varepsilon_2 \right)^2 + (\varepsilon_1 \Gamma_2 + \varepsilon_2 \Gamma_1)^2 \right]^{1/2}}, \quad (21)$$

$$\theta(V_g) = \arctan \left[\frac{\varepsilon_1 \Gamma_2 + \varepsilon_2 \Gamma_1}{\varepsilon_1 \varepsilon_2 - \left(\sqrt{\Gamma_1^L \Gamma_2^R} - s \sqrt{\Gamma_1^R \Gamma_2^L} \right)^2} \right] \bmod \pi, \quad (22)$$

with $\Gamma_j = \sum_l \Gamma_j^l$. For later use we define

$$\Gamma = \sum_{j,l} \Gamma_j^l. \quad (23)$$

For a fixed set of Γ_j^l the δ dependence of $|t(V_g)|$ and $\theta(V_g)$ is shown in the first columns of Figs. 1 and 2 for $U/\Gamma = 0.2$. The results are qualitatively the same as those obtained for $U = 0$. For generic level-lead couplings Γ_j^l the gate voltage dependence of Eq. (21) in the limit of small and large δ/Γ is dominated by two peaks (of height ≤ 1) and a transmission zero. Associated with the transmission zero is a π phase lapse at the same gate voltage. The transmission zero (and phase lapse) follows from perfect destructive interference at a particular V_g and in the limit of a strong asymmetry in the coupling of the two levels to the leads, $\Gamma_1 \ll \Gamma_2$ or vice versa, can be understood as resulting from a Fano anti-resonance [20]. Apparently the Fano anti-resonance with vanishing transmission is robust if one goes away from this limit towards more symmetric level-lead couplings. Across each of the transmission resonances θ increases roughly by π as expected for a Breit-Wigner resonance. Further details of $|t(V_g)|$ and $\theta(V_g)$ depend on s . For $s = +$ the transmission zero (and phase lapse) is located between the two conductance peaks for all δ . For $\delta \rightarrow 0$ the resonance peak positions depend on the asymmetry of the Γ_j^l and the separation of the peaks is small if the Γ_j^l are close to l-r symmetry, that is close to $\Gamma_j^L = \Gamma_j^R$. For l-r symmetric dots and $\delta = 0$ the transmission zero (and phase lapse) disappears (not shown in the figures). This is an example of a submanifold in parameter space with nongeneric behavior. A complete account of such cases (which also remain nongeneric for $U > 0$) is given in Refs. [12] and [13]. As they require fine tuning these parameter sets are presumably irrelevant in connection with the experiments and we will here only briefly mention results obtained in such cases.

For $s = -$ and fixed Γ_j^l the position of the transmission zeros and phase lapses with respect to the CB peaks is different for small or large δ/Γ (see Fig. 2). At small δ/Γ it is located between the two conductance peaks, whereas for large δ/Γ it lies on one of the outer sides of these peaks [9]. In the crossover regime between these limiting cases the height of one of the peaks decreases, while the other becomes broader and splits up into two resonances separated by a minimum with non-vanishing conductance [see Fig. 2 (g) and (j)]. The crossover scale δ_c depends on the choice of Γ_j^l . For large δ/Γ , $|t|$ has three local maxima, although the height of one of the maxima is significantly smaller than the height of the other two (not shown in Fig. 2). For fixed, asymmetric Γ_j^l and $\delta \rightarrow 0$ the separation of the two conductance peaks for $s = -$ is significantly larger than for $s = +$ [compare Figs. 1 (a) and 2 (a)].

It is important to note that for small δ/Γ essential features of the universal phase lapse regime established in the experiments are already found at $U = 0$: regardless of the sign s for generic Γ_j^l (that is with the exception of a few cases with increased symmetry) two transmission resonances are separated by a transmission zero and π phase lapse. At $U = 0$ the peak separation is too small and the shape of the V_g dependence of the transmission and phase close to the peaks is qualitatively different from those observed experimentally (namely Lorentzian-like for the magnitude of the transmission, s-shaped for the phase). As we show next the latter problems do not arise for sufficiently large interaction U , which in particular leads to an increased separation $U + \delta$ of the transmission peaks.

4. Results: Spin-polarized dots

4.1. The generic phase lapse scenario

In Ref. [19] it was shown that fRG and NRG results for $|t(V_g)|$ and $\theta(V_g)$ agree quantitatively up to fairly large U . For a generic set of couplings γ we present fRG data for $\theta(V_g)$ and $|t(V_g)|$ together with the occupancies of the levels n_j for different U and δ in Figs. 1 ($s = +$) and 2 ($s = -$). Increasing U/Γ the separation of the transmission peaks in the limit of small and large δ/Γ increases and is eventually given by $U + \delta$. Even though this charging effect appears to be straightforward it is important to note that in particular the groundstate at small δ/Γ is highly correlated. This becomes explicit from the mapping of the present problem on a generalized single impurity Anderson and Kondo model as discussed in Ref. [13]. An indication of strong correlation effects are the correlation-induced resonances of the transmission found in Ref. [12], which we briefly mention below. With increasing U , even at small δ/Γ the gate voltage dependence of $\theta(V_g)$ across the transmission resonances becomes s-shaped and the resonances more Lorentzian-like [see third columns of Figs. 1 and 2]. Obviously, for $s = +$ the transmission zero and phase lapse remain between the two transmission peaks for all δ and U (see Fig. 1). For $s = -$ this only holds for sufficiently small level spacings as, similar to the $U = 0$ case, with increasing δ/Γ a crossover sets in to a regime in which the transmission zero and phase lapse are no longer between the peaks. Analogously to the $U = 0$ case, the crossover scale δ_c depends on the particular choice of Γ_j^l . As can be seen from the second row of Fig. 2 (the CB peaks at large U have still almost equal height), with increasing U/Γ , δ_c is pushed towards larger values. The Coulomb interaction thus stabilizes the parameter regime of universal phase lapses. This shows that the effect of the Coulomb interaction leading to universal π phase lapses between separated CB peaks in a two-level dot is rather straightforward: for small δ/Γ the phase lapse and transmission zero are already present at $U = 0$, and the effect of finite U is simply that the CB peaks become well separated because of charging effects. They also lead to a Lorentzian-like lineshape of the peaks and an s-like variation of θ across them.—The present scenario has to be contrasted to the one obtained for $N > 2$ levels discussed in Ref. [19]. The generic appearance of $N - 1$ transmission zeros and phase lapses separating the transmission peaks at small δ/Γ and $U = 0$ is specific to the case with $N = 2$ levels. For $N > 2$ the number of transmission zeros and phase lapses at $U = 0$ strongly depends on the parameters and the mechanism leading to universal π phase lapses at sufficiently large U (at small δ/Γ) is much more involved [19]. This shows that although important insights can be gained from studying two-levels to achieve a *complete* understanding of the phase lapse scenario it is essential to study dots with Coulomb interaction and more than two levels [19].

The lineshape of $|t|$ shows characteristic differences in the limits of small and large δ/Γ . In the universal regime at small δ/Γ and for sufficiently large U/Γ the two CB peaks have equal width of order Γ (not Γ_j) and equal height which is consistent with the expectation that at each peak the transport occurs through both bare levels

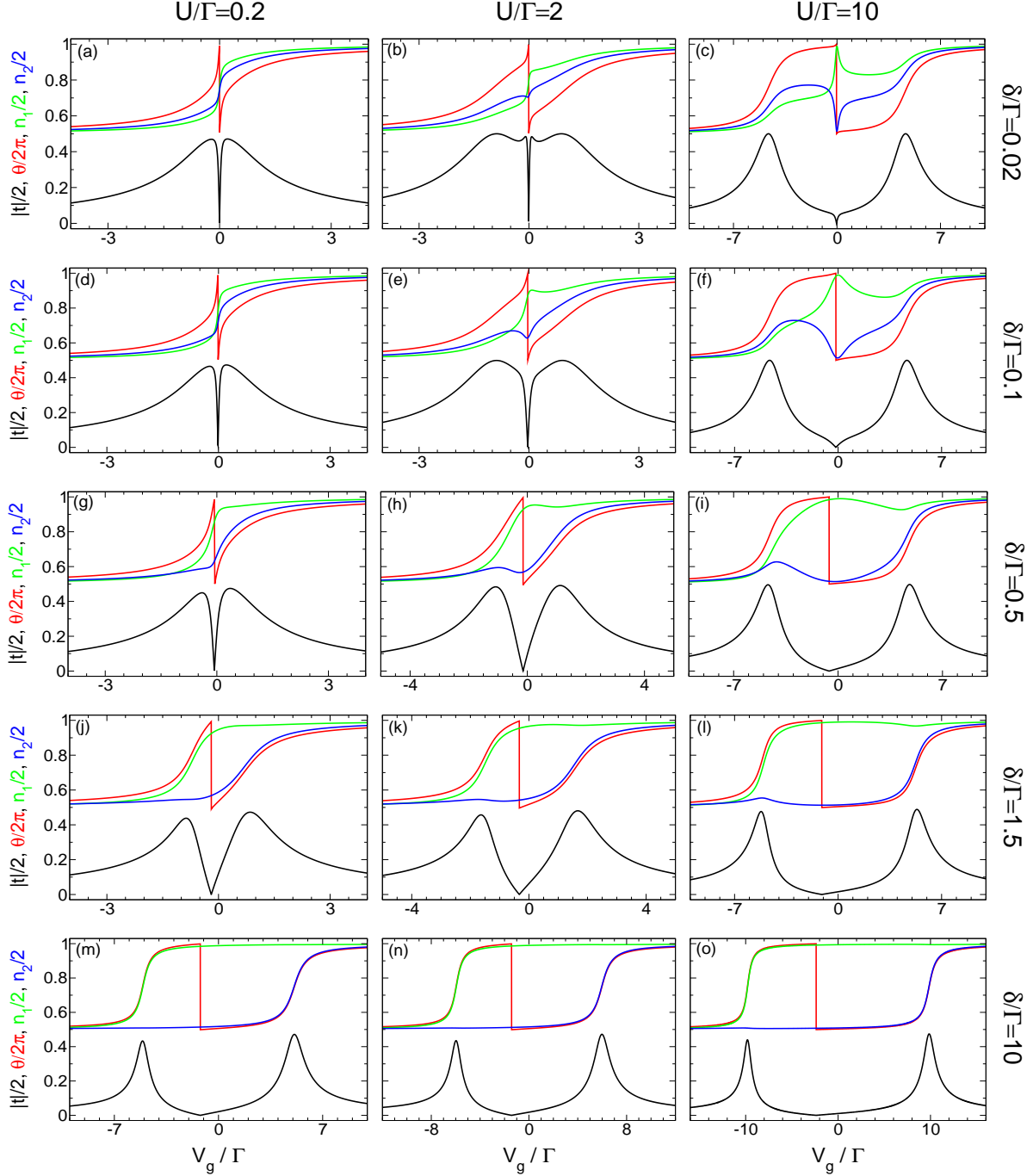


Figure 1. Systematic account of the energy scales U/Γ and δ/Γ that govern the gate voltage V_g dependence of the magnitude of the transmission $|t|$ (black), the transmission phase θ (red) and the level occupancies (green and blue) of a spin-polarized two-level dot at $T = 0$. The parameters are $\gamma = \{0.1, 0.3, 0.4, 0.2\}$ and $s = +$. For better visibility $n_{1/2}$ were shifted by 1. The depicted behavior is the generic one and in particular qualitatively independent of the actual choice of γ (up to certain cases of increased symmetry; for examples see the text). The behavior at $U/\Gamma = 0.2$ is qualitatively the same as the one at $U = 0$. The results were obtained using the truncated fRG.

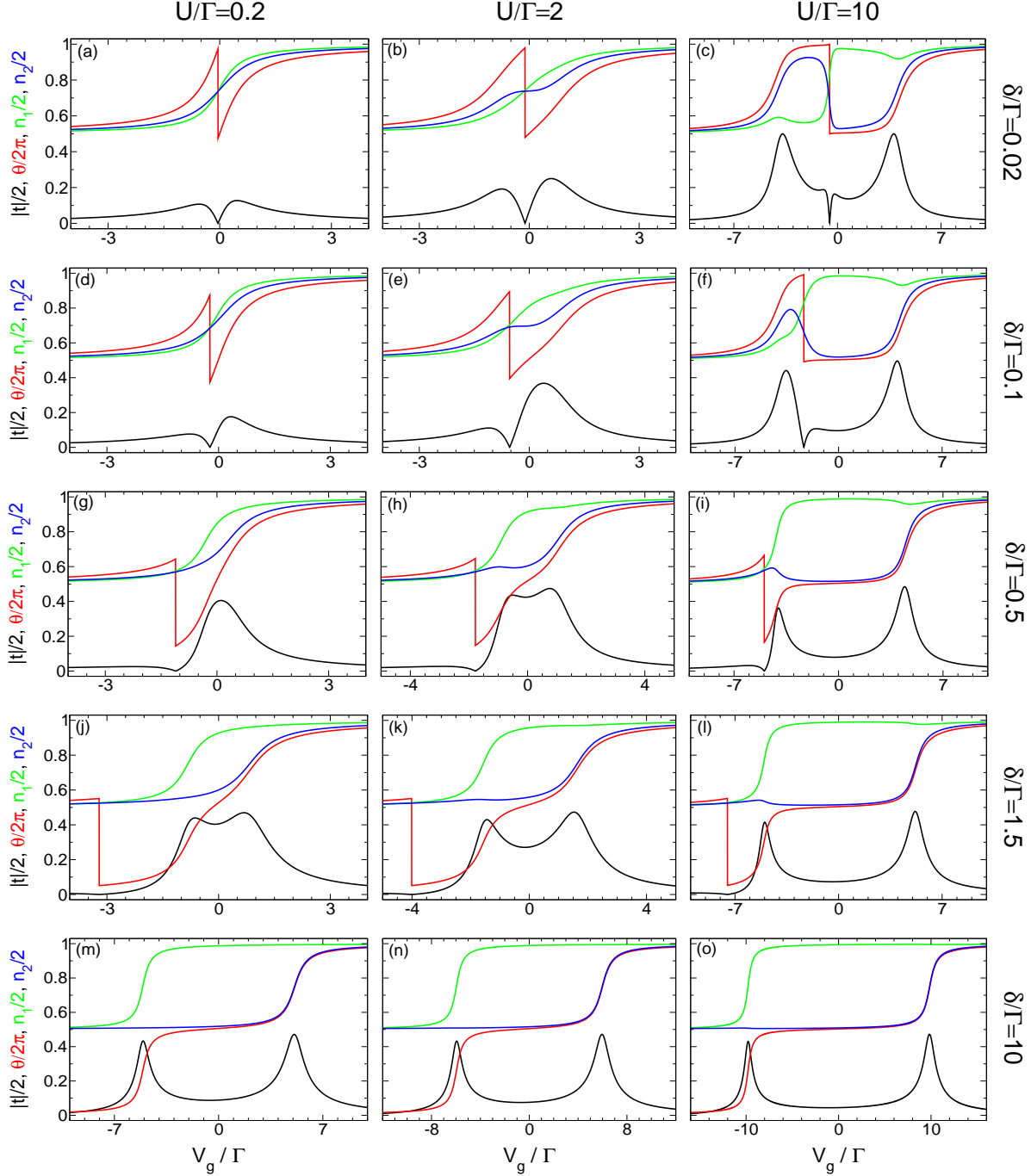


Figure 2. The same as in Fig. 1, but for $s = -$.

simultaneously. A similar behavior is observed in the experiments. In the mesoscopic regime ($\delta/\Gamma \gg 1$) the width of the j 'th peak is given by Γ_j and the relative height h_j by Γ_j^L/Γ_j^R , independent of the value of U . This effectively noninteracting lineshape can be understood from the gate voltage dependence of the effective level positions $\varepsilon_j^{\Lambda=0}$ at the end of the fRG flow. When one level is charged the effective level position of the other level is pushed downwards by U . Besides this, the gate voltage dependence of the $\varepsilon_j^{\Lambda=0}$ remains linear, leading to two transmission peaks at gate voltages $\varepsilon_j^{\Lambda=0}(V_g) = 0$

with separation $U + \delta$, but with the same width and height as for $U = 0$. The hopping between the two effective levels generated in the fRG flow is small and can be neglected.

Apart from the CB peaks, for sufficiently large U/Γ the transmission shows additional features at small V_g/Γ [see Figs. 1 (b), (c), (e) and 2 (c)]. These are the correlation-induced resonances mentioned in the introduction, which have been found to be most pronounced at $\delta = 0$ and in this case occur for interactions larger than a critical U_c which depends on the Γ_j^l and s [12, 13]. Their appearance indicates that the groundstate at small δ/Γ is strongly correlated (as mentioned in Ref. [12] the correlation-induced resonances are not captured by a mean-field analysis; see below). Associated with the correlation-induced resonances is a sharp increase of θ [see Figs. 1 (b) and (e)]. At large U/Γ the correlation-induced resonances are exponentially (in U/Γ) sharp features that vanish quickly with increasing T (see below), which might be one of the reasons why up to now they have not been observed in experiments. The correlation-induced resonances are not directly linked to the universal phase lapse scenario.

For increasing U/Γ at fixed δ/Γ and decreasing δ/Γ at fixed U/Γ we observe an increased tendency towards population inversion of the n_j . We define that a population inversion occurs if (1) $n_1(V_g^{\text{PI}}) = n_2(V_g^{\text{PI}})$ at a certain V_g^{PI} and (2) one n_j has positive and one negative slope at V_g^{PI} so that the filling of one level causes a tendency for the other to empty. For large U/Γ and small δ/Γ it is mainly the more strongly coupled level (in Figs. 1 and 2, this is the level 2 shown in blue) whose population increases across both CB peaks while it is depopulated in between. This behavior is reminiscent of the one discussed in the model with a broad and several narrow levels [3], where a relation between population inversion and phase lapse behavior was proposed. Remarkably, for sufficiently large U/Γ , we find population inversion even for small asymmetries Γ_2/Γ_1 (which is only 1.5 in the example of Figs. 1 and 2). We emphasize that despite this resemblance to the observation of Ref. [3], the $N = 2$ model is not appropriate to establish a general relation between the appearance of population inversions and π phase lapses at small δ/Γ [10, 6]. While the latter are already present at $U = 0$, the former only develop with increasing U [compare Figs. 1 (a), (d) or 2 (a), (d) to Figs. 1 (c), (f) or 2 (c), (f)]. Note that the gate voltage V_g^{PI} at which the population inversion occurs is generically *not* identical to the position of the phase lapse and transmission zero [see Figs. 1 (b), (c), (f) and 2 (c), (f)] [13]. However, for l-r symmetric Γ_j^l Eq. (9) ensures that if a population inversion occurs its position is identical to the one of the phase lapse and transmission zero.

As can be seen in Figs. 1 (c), (f) and 2 (c), (f) for small δ/Γ and large U/Γ the n_j show a rather strong gate voltage dependence between the CB peaks. Nevertheless the total dot occupancy $n_1 + n_2$ is only weakly V_g dependent and close to 1 within the entire CB valley. This is reminiscent of the plateau-like occupancy in the local moment regime of the single impurity Anderson model showing the Kondo effect. As discussed in Ref. [13] a relation to this model can indeed be established.

We note in passing that with the exception of the nongeneric case of l-r symmetric Γ_j^l , $s = +$ and $\delta = 0$, the n_j are continuous functions of V_g .

4.2. Comparison to mean-field theory

In Refs. [10] and [11] Golosov and Gefen (GG) analyze the phase lapse scenario of the spin-polarized interacting two-level dot within the mean-field approximation. However, they anticipated themselves that quantum fluctuations not captured in the mean-field approach could be important. Examples of this had been pointed out already in Refs. [5] and [12]. Thus, GG emphasized that the effects of such fluctuations on their results need to be studied in subsequent work. The present subsection is devoted to this task.

GG consider the subspace of level-lead couplings defined by $\Gamma_1^L - \Gamma_1^R = \Gamma_2^R - \Gamma_2^L$. Performing a unitary transformation on the dot states the part of the Hamiltonian Eq. (1) containing dot operators can be transformed to (see Refs. [10] and [11])

$$H_{\text{dot}} + H_{\text{lead-dot}} = \sum_{j=1,2} \hat{\varepsilon}_j \hat{d}_{j,\sigma}^\dagger \hat{d}_{j,\sigma} + U \hat{d}_1^\dagger \hat{d}_1 \hat{d}_2^\dagger \hat{d}_2 - \hat{t}(\hat{d}_1^\dagger \hat{d}_2 + \text{H.c.}) \\ - \left[c_{0,L} \left(\hat{t}_1 \hat{d}_1^\dagger + \hat{t}_2 \hat{d}_2^\dagger \right) + c_{0,R} \left(\hat{t}_1 \hat{d}_1^\dagger - \hat{t}_2 \hat{d}_2^\dagger \right) + \text{H.c.} \right], \quad (24)$$

with the transformed operators and parameters indicated by a hat. The change of basis leads to a direct hopping \hat{t} between the transformed levels. We here focus on the relative sign $\hat{s} = -$. GG then introduce the two new dimensionless parameters κ and α as $\hat{t} = -\kappa\hat{\delta}/(2\sqrt{1-\kappa^2})$ and $\alpha = (|\hat{t}_1| - |\hat{t}_2|)/\sqrt{\hat{t}_1^2 + \hat{t}_2^2}$. Varying κ and α GG investigate the phase lapse behavior for fixed level spacing (in the new basis) $\hat{\varepsilon}_2 - \hat{\varepsilon}_1 = \hat{\delta} = 0.256\hat{\Gamma}$ and interaction $U/\hat{\Gamma} = 6.4$. As the parameters in the new basis are rather complicated combinations of the original ones, the variation of α and κ corresponds to the variation of the Γ_j^l (within the above specified subspace), δ and even s . Our simple picture that increasing the level spacing δ of the untransformed model leads from the universal to the mesoscopic regime cannot easily be made explicit using the parameters of GG. To make the comparison of our results to the mean-field study definite we nevertheless follow the steps of GG.

Varying $\alpha, \kappa \in [0, 1[$ at $\hat{s} = -$ we move around in the right part of what is called the “phase diagram” by GG (Fig. 4 of Ref. [11]). In Fig. 3 we show the behavior of $|t|$ and θ varying α at fixed κ [Figs. 3 (a)-(d)] and κ at fixed α [Figs. 3 (e)-(h)], respectively. In the first case, upon increasing α at constant $\kappa = 0.5$, we move from GGs “phase 2”, (red in Fig. 4 of Ref. [11]), with the transmission zero and phase lapse outside the two CB peaks, into “phase 1” (blue in Fig. 4 of Ref. [11]), with the transmission zero and phase lapse between the peaks. The mean-field approximation correctly captures the presence of these two regimes. We find a smooth crossover between them (which is why we prefer the notion of different “regimes” rather than “phases”): the V_g value at which the transmission zero and phase lapse occur *smoothly* crosses from lying outside the right CB peak to lying between the two CB peaks. This is similar to the smooth crossover we observe in the $s = -$ case of the untransformed model when moving from the mesoscopic to the universal regime (see columns of Fig. 2).

For fixed $\alpha = 0.6$ and increasing κ we move from “phase 3” (green in Fig. 4 of Ref. [11]) into “phase 1”. In contrast to the mean-field approximation where an abrupt

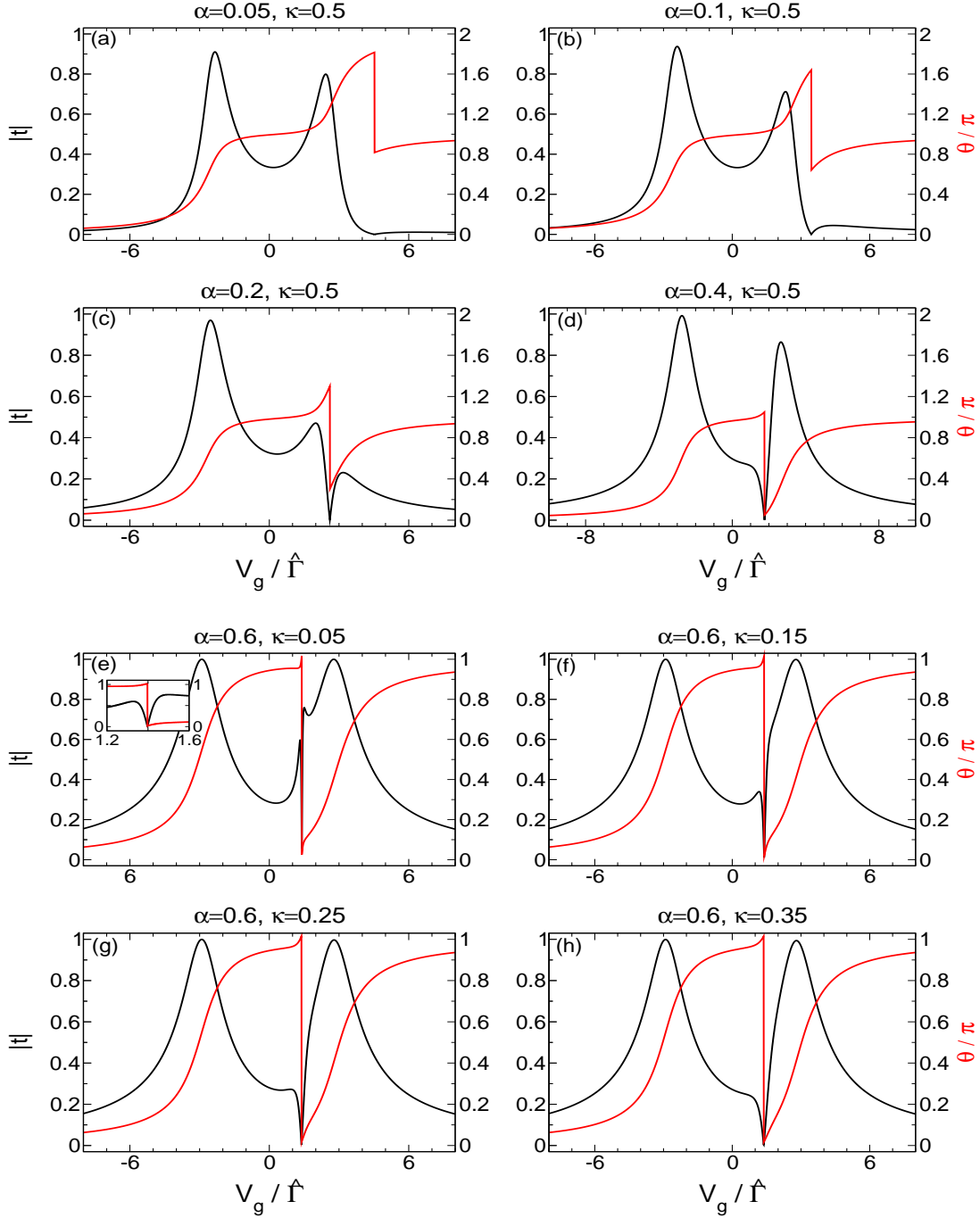


Figure 3. Two traces through the mean-field “phase diagram” of GG. Figures (a)-(d) are for constant κ and different α moving from GGs “phase” 2 into “phase” 1. Figures (e)-(h) are for constant α and different κ moving from GGs “phase 3” into “phase 1”. The inset in Fig. (e) shows a zoom in of the gate voltage region around the phase lapse. For a detailed comparison to the mean-field results see the text. The results were obtained at $T = 0$ using the truncated fRG.

transition from “phase 3” to “phase 1” occurs, Figs. 3 (e)-(h) show a rather smooth evolution. The mean-field “phase 3” is characterized by discontinuous population switching and a phase lapse between the CB peaks which, surprisingly, is smaller

than π [10, 6]. Furthermore, in this parameter regime the mean-field results show no transmission zero, as discussed in Ref. [6]. However, from Figs. 3 (e)-(h) it is apparent that “phase 3”, is an artifact of the mean-field approximation: upon taking fluctuations into account via fRG, the π phase lapse and the transmission zero are found to remain in the CB valley. The evolution with increasing κ is similar to the $s = +$ case of the untransformed model when the level spacing is increased at fixed Γ_j^l (see the second and third columns of Fig. 1). “Phase 3” then corresponds to the parameter regime with small level spacing and a sizable U/Γ in which correlations are of particular importance leading e.g. to the correlation-induced resonances [see Figs. 3 (e)-(h)]. That the mean-field approximation fails to properly describe this strongly correlated regime is not surprising and has been recognized earlier [12]. In Ref. [13] a connection between the small δ regime of the present model and the local moment (Kondo) regime of the single-impurity Anderson model was established. Thus, the artifacts of the mean-field approximation for the spinless two-level dot are reincarnations of the the well-known artifacts it produces when applied to the Anderson model in the local moment regime.

Upon taking fluctuations into account, the discontinuities of the $n_{1/2}$ in “phase 3” are washed out. The only choice of parameters for which we find discontinuous behavior is the one with l-r symmetric Γ_j^l , $s = +$ and $\delta = 0$, a case which was already identified as being nongeneric [12]. Any arbitrarily small deviation from these conditions leads to a continuous gate voltage dependence of $n_{1/2}$. For parameters close to the nongeneric point the change in n_j at first sight appears to be rather sharp and an extremely high resolution in V_g is required to identify the behavior as continuous.

The fact that the mean-field treatment at $U > 0$ and small level spacings incorrectly causes the transmission zero to disappear and the corresponding phase lapse to become smaller than π is its most consequential problem. By generating such features, the mean-field treatment masks the very simple scenario that emerges upon properly including fluctuations: for increasing U , the π phase lapse and transmission zero found for small δ/Γ at $U = 0$ remain in the CB valley, while the transmission peaks become well separated, Lorentzian-like and the phase acquires an s-shape across the resonances.

4.3. Finite temperatures

We next investigate how the phase and magnitude of the transmission are affected by finite temperatures. To this end, we use the new FDM-NRG algorithm recently proposed in Ref. [26]. In Fig. 4 we show NRG data for $|t(V_g)|$ and $\theta(V_g)$ at different T . We consider generic level-lead couplings $\gamma = \{0.27, 0.33, 0.16, 0.24\}$, $U/\Gamma = 10$, $s = \pm$ and $\delta/\Gamma = 0.02$ (universal regime) as well as $\delta/\Gamma = 4$ (mesoscopic regime). As expected, with increasing temperature the sharp π phase lapses are gradually smeared out, the transmission zero vanishes and the change of θ at the phase lapse becomes smaller than π . Furthermore, the CB peaks decrease and broaden. For $\delta/\Gamma = 4$ and $s = -$ [Fig. 4 (d)] the phase lapse lies outside the CB peaks and outside the window of gate voltages shown.

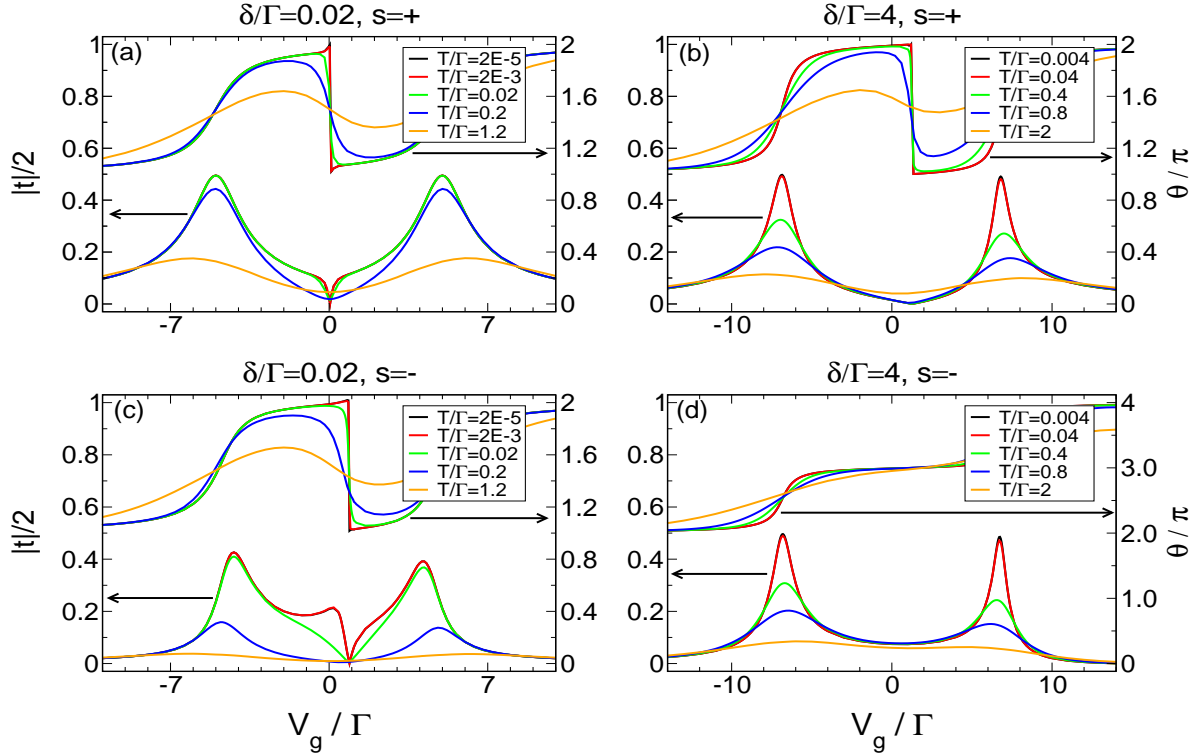


Figure 4. Temperature dependence of $|t(V_g)|$ and $\theta(V_g)$ obtained by NRG for $\gamma = \{0.27, 0.33, 0.16, 0.24\}$, $U/\Gamma = 10$ for $s = \pm$ and in the universal ($\delta/\Gamma = 0.02$) and the mesoscopic ($\delta/\Gamma = 4$) regime. We used the NRG parameters $\Lambda_{\text{NRG}} = 2.3$ and $N_{\text{kept}} \sim 512$.

In the mesoscopic regime [Figs. 4 (b) and (d)] the explicit temperature dependence of the Green function entering Eq. (6) via Eq. (7) is rather weak and the temperature dependence of the CB peaks and the phase lapse can be understood from the behavior in the noninteracting model, but with level spacing $U + \delta$. For small T the height $h_j(T)$ of the j 'th CB peak scales as $1 - h_j(T)/h_j(0) \sim T^2/\Gamma_j^2$ and the width w of the phase lapse as $w \sim T^2/(\delta + U)^2$ [9]. The relevant scale for sizable temperature effects in the peak height is thus Γ_j while it is $U + \delta$ in the smearing of the phase lapses. Since we have chosen $\Gamma_j \ll \delta + U$ a reduction of h_j is visible for temperatures at which the phase lapse is still fairly sharp [see Fig. 4 (b)].

Due to the importance of correlation effects at small δ/Γ , the T dependence of $|t(V_g)|$ and $\theta(V_g)$ in the universal regime is different from the noninteracting case. Here the explicit temperature dependence of \mathcal{G} is much stronger and cannot be neglected. The resulting T dependence of $|t(V_g)|$ and $\theta(V_g)$ is shown in Figs. 4 (a) and (c). A comparison to Fig. 4 (b) shows that in the universal regime the smearing of the phase lapse sets in at a lower energy scale than in the mesoscopic regime. This scale depends on the relative sign s of the level-lead hopping matrix elements [compare Figs. 4 (a) and (c)]. Furthermore, in contrast to the mesoscopic regime the scales on which the CB peaks and the phase lapse are affected by temperature are comparable. A more detailed investigation of the temperature dependence in the universal regime, which

also discusses the fate of the correlation-induced resonances, is beyond the scope of the present work and is left as subject for future studies.

5. Results: Spin-degenerate dots

We finally investigate the effect of the spin degree of freedom on the discussed phase lapse scenario, at $T = 0$. In Figs. 5 ($s = +$, $U/\Gamma = 3$) and 6 ($s = -$, $U/\Gamma = 4$) we show fRG data for the evolution of $|t(V_g)|$, $\theta(V_g)$ and $n_j(V_g)$ (for a fixed spin direction) with increasing δ for a generic $\gamma = \{0.1, 0.2, 0.5, 0.2\}$. The overall dependence of $\theta(V_g)$ on δ is similar to the one observed in the spinless case (compare to Figs. 1 and 2). In particular, the behavior at small δ/Γ appears to be almost unaffected by the presence of the spin degree of freedom [Figs. 5 (a), (b) and 6 (a), (b)]. For large δ/Γ [Figs. 5 (d) and 6 (d)] the transmission resonances are located at odd average total filling of the two-level dot indicated by shoulders in the n_j [Figs. 5 (d) and 6 (d)]. At these fillings and for sufficiently large U/Γ the Kondo effect is active and the resonances cannot be regarded as Lorentzian-like CB peaks. Instead they show a plateau-like shape known from the spinful single-level dot (see Ref. [27] and references therein). Across the Kondo plateaus of $|t|$ the s-shaped increase of the phase is interrupted by a shoulder at $\theta \approx \pi/2$ as expected for the Kondo effect [27]. It would be very interesting to study how each of the Kondo plateaus of $|t|$ with increasing temperature crosses over to two CB peaks and the phase behaves in the generated CB valley. This question is left for future investigations.

The behavior of the phase in the presence of the Kondo effect was experimentally investigated at temperatures comparable to the Kondo temperature [21], and much below the Kondo temperature [22]. As we study the zero temperature case it is proper to compare our calculations to the measurements at low temperatures. Indeed Fig. 6 (c) for intermediate δ/Γ qualitatively reproduces the experimental results at low temperature as shown in Fig. 3 c of Ref. [22]. In particular the increase of the phase by more than π and the absence of clearly developed Kondo plateaus are reproduced.

In Fig. 5 (a) we left out the fRG data around $V_g = 0$ as for these gate voltages some of the components of the flowing two-particle vertex become large. This indicates the breakdown of our present truncation scheme [24, 25] and the results for $|t|$, θ and n_j become unreliable. For an explicit comparison to NRG data of $|t|$ see Fig. 7 (a). We note in passing that for $s = +$ correlation-induced resonances occur also in the model with spin [Fig. 5 (a)] [24].

In Fig. 7 we compare fRG and NRG results for l-r symmetric level-lead couplings. The computational resources required to obtain NRG data away from l-r symmetry become large and such data are not required for the aim of the present paper. We can then use Eq. (9) and must only compute the occupancies n_j , which is numerically less demanding. For $\delta > 0$ (as exclusively shown) it is only the absence of the correlation-induced resonances for $s = +$ [compare Figs. 5 (a) and 7 (a)] which is different from the results of the generic γ shown in Figs. 5 and 6. With the exception of the $V_g \approx 0$

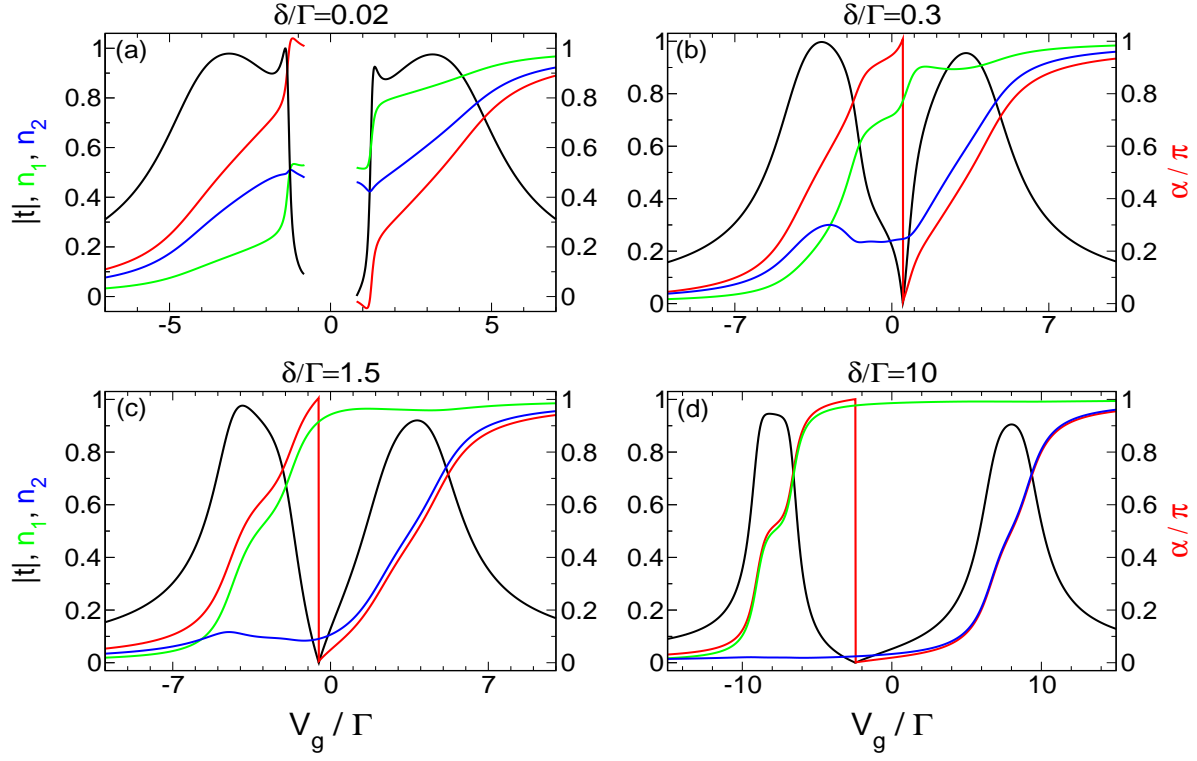


Figure 5. Gate voltage V_g dependence of $|t|$ (black), θ (red) and the level occupancies per spin direction (green and blue) of a spinful two-level dot at $T = 0$ for different δ obtained by fRG. The parameters are $U/\Gamma = 3$, $\gamma = \{0.1, 0.2, 0.5, 0.2\}$ and $s = +$. In (a), no data are shown around $V_g = 0$ for reasons explained in the text.

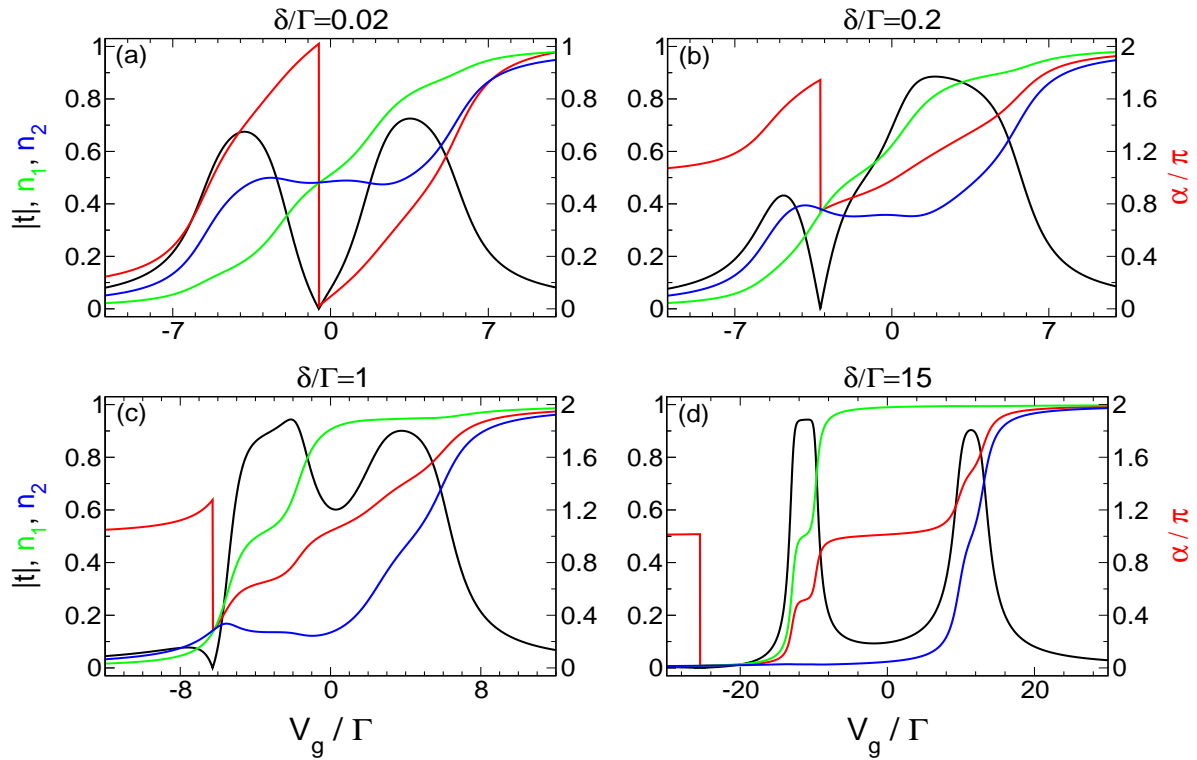


Figure 6. The same as in Fig. 5, but for $U/\Gamma = 4$ and $s = -$.

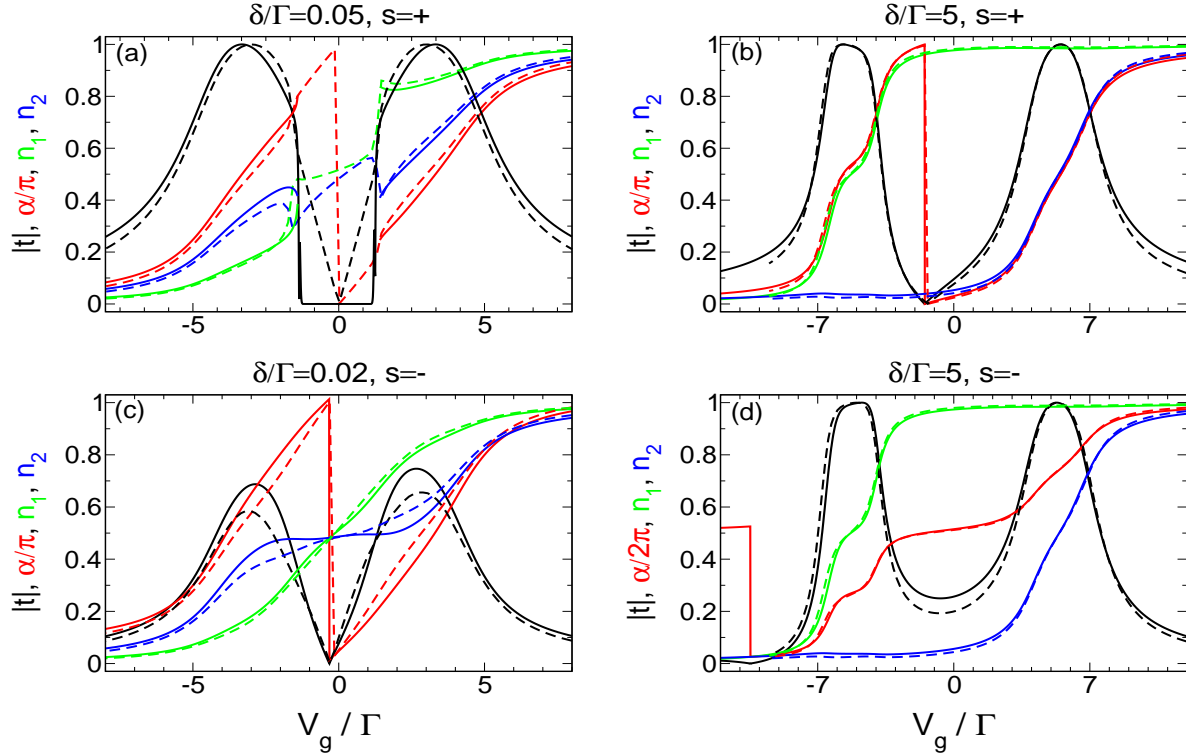


Figure 7. Comparison of fRG (solid) and NRG (dashed) data for $|t(V_g)|$, $\theta(V_g)$ and $n_j(V_g)$ (per spin direction) in the universal (small δ/Γ) and mesoscopic regime (large δ/Γ) of a spinful two-level dot at $T = 0$. The parameters are $U/\Gamma = 3$ and $\gamma = \{0.15, 0.15, 0.35, 0.35\}$. In (a) the fRG data for $\theta(V_g)$ and $n_j(V_g)$ around $V_g = 0$ are not shown. Already the unsatisfactory comparison between fRG and NRG for $|t|$ indicate that the fRG becomes unreliable in this regime. For more details on this, see the text. For the NRG parameters we used $\Lambda_{\text{NRG}} = 2.5$, $N_{\text{kept}} = 1024$ for $s = +$ and $N_{\text{kept}} = 2048$ for $s = -$.

regime in the case of small δ and $s = +$ the fRG and NRG data compare quite well. In this case we only show the fRG data for $|t|$ as the results for the phase and occupancies become rather erratic. The reason for the breakdown of the currently used truncated fRG is explained in Refs. [24] and [25] and is related to the fact that at small δ and small V_g the correlations in effect become extremely large.

6. Summary

In the present paper we studied the appearance of phase lapses in an interacting two-level quantum dot considering the entire parameter space using NRG and a truncated fRG scheme.

As a starting point we briefly discussed the noninteracting case at temperature $T = 0$ and pointed out that for generic level-lead couplings, that is up to cases with increased symmetry, essential features of the universal phase lapse scenario are already established at $U = 0$. For single-particle level spacings δ small compared to the level

broadenings Γ_j the transmission is characterized by two transmission peaks of equal width with a transmission zero and an associated π phase lapse between them (universal regime). For large δ/Γ at $U = 0$ the appearance or not of a transmission zero and phase lapse between the two transmission peaks depends on the relative sign s of the level-lead couplings (mesoscopic regime). Within a spinless model we have shown that the separation of the two transmission peaks increases linearly with the interaction U while the π phase lapse and transmission zero remain in the valley between them. Furthermore, with increasing U the increase of the phase across the peaks takes an s-shape and the peaks become Lorentzian-like, thus assuming shapes resembling those observed experimentally [14, 15, 16]. For $s = -$ and increasing δ , a crossover occurs to a regime in which the π phase lapse and transmission zero lies outside the two CB peaks. The crossover scale δ_c increases with increasing interaction and thus the Coulomb repulsion stabilizes the universal phase lapse behavior. We have investigated the relation between phase lapses and population inversions of the level occupancies n_j .

We have shown that a mean-field treatment of the present problem correctly reproduces certain features of the behavior discussed above, but is not able to produce the universal phase lapse scenario at small δ/Γ due to artifacts of the approximation such as a phase lapse by less than π [10, 11] and a vanishing of the transmission zero [6]. Furthermore, the discontinuous gate voltage dependence of the n_j found in the mean-field approximation turned out to be an artifact.

Next, we studied how the phase lapse behavior is affected by temperatures $T > 0$. The universal phase lapse (at small δ/Γ) is smeared out but remains visible for not too large T . In the mesoscopic regime with $\delta/\Gamma \gg 1$ the smearing of the phase lapse and the decrease of the CB peaks can be understood in detail in analogy to the noninteracting case. For $\delta/\Gamma \ll 1$ correlations are more important and a detailed understanding of the temperature dependence of the transmission $t(V_g)$ requires further studies.

The phase lapse behavior in both the universal and mesoscopic regimes is also stable if the spin degree of freedom is included. For sufficiently large U/Γ in this case the Kondo effect is active at odd average dot filling, leading to minor modifications of the scenario discussed above. In particular, at large δ/Γ the $T = 0$ transmission peaks are Kondo plateaus rather than Lorentzian-like CB peaks. Across these Kondo plateaus the phase shows a shoulder at $\theta \approx \pi/2$. In contrast, the behavior at small δ/Γ appears to be almost unaffected by the spin degree. A study of the combined effect of finite temperature and spin is left for future work.

Acknowledgments

We thank R. Berkovits, P. Brouwer, Y. Gefen, L. Glazman, D. Golosov, M. Heiblum, J. Imry, V. Kashcheyevs, J. König, F. Marquardt, M. Pustilnik, H. Schoeller, K. Schönhammer, and A. Silva for valuable discussions. This work was supported in part, for VM, by the DFG through SFB602; for TH, AW and JvD by the DFG through SFB631 and De730/3-2, and also by Spintronics RTN (HPRN-CT-2002-00302), NSF

(PHY99-07949) and DIP-H.2.1; and for YO by DIP-H.2.1, BSF and the Humboldt foundation.

References

- [1] Sohn L L, Kouwenhoven L P and Schön G (eds) 1997 *Mesoscopic Electron Transport* (Kluwer, Dordrecht).
- [2] Kouwenhoven L P and Glazman L 2001, *Phys. World* **14**(1) 33
- [3] Silvestrov P G and Imry Y 2000 *Phys. Rev. Lett.* **85** 2565; Silvestrov P G and Imry Y 2001 *Phys. Rev. B* **65** 035309
- [4] König J and Gefen Y 2005 *Phys. Rev. B* **71** 201308(R)
- [5] Sindel M, Silva A, Oreg Y and von Delft J (2005) *Phys. Rev. B* **72** 125316
- [6] Goldstein M and Berkovits R (2006) cond-mat/0610810.
- [7] Hackenbroich G (2001) *Phys. Rep.* **343** 463
- [8] Gefen Y. 2002 in *Quantum Interferometry with Electrons: Outstanding Challenges* Lerner I V et al. (eds) (Kluwer, Dordrecht) p. 13.
- [9] Silva A, Oreg Y and Gefen Y (2002) *Phys. Rev. B* **66**, 195316
- [10] Golosov D I and Gefen Y (2006) *Phys. Rev. B* **74**, 205316
- [11] Golosov D I and Gefen Y (2007) *New J. Phys.* this issue, p.
- [12] Meden V and Marquardt F (2006) *Phys. Rev. Lett.* **96** 146801
- [13] Kashcheyevs V, Schiller A, Aharony A and Entin-Wohlman O (2006) cond-mat/0610194
- [14] Yacoby Y, Heiblum M, Mahalu D and Shtrikman H (1995) *Phys. Rev. Lett.* **74** 4047
- [15] Schuster R, Buks E, Heiblum M, Mahalu D, Umansky V and Shtrikman H (1997) *Nature* **385** 417
- [16] Avinun-Khalish M, Heiblum M, Zarchin O, Mahalu D and Umansky V (2005) *Nature* **436** 529
- [17] Aharony A, Entin-Wohlman O, Halperin B and Imry Y (2002) *Phys. Rev. B* **66** 115311
- [18] Berkovits R, von Oppen F and Kantelhardt J W (2004) *Euro. Phys. Lett.* **68** 699
- [19] Karrasch C, Hecht T, Oreg Y, von Delft J and Meden V (2006) cond-mat/0609191
- [20] Fano U (1961) *Phys. Rev.* **124** 1866
- [21] Ji Y, Heiblum M, Sprinzak D, Mahalu D and Shtrikman H (2000) *Science* **290** 779
- [22] Ji Y, Heiblum M and Shtrikman H (2002) *Phys. Rev. Lett.* **88** 076601
- [23] Krishna-murthy H R, Wilkins J W and Wilson K G (1980) *Phys. Rev. B* **21** 1003
- [24] Karrasch C, Enss T and Meden V (2006) *Phys. Rev. B* **73** 235337
- [25] Karrasch C (2006) Diploma-thesis, Universität Göttingen; cond-mat/0612329
- [26] Weichselbaum A and von Delft J (2006) cond-mat/0607497
- [27] Gerland U, von Delft J, Costi T A and Oreg Y (2000) *Phys. Rev. Lett.* **84** 3710
- [28] Salmhofer M and Honerkamp C (2001) *Prog. Theor. Phys.* **105** 1
- [29] Hedden R, Meden V, Pruschke Th and Schönhammer K (2004) *J. Phys.: Condens. Matter* **16** 5279
- [30] Meden V, lecture notes on the “Functional renormalization group”, <http://www.theorie.physik.uni-goettingen.de/~meden/funRG/>
- [31] Negele J W and Orland H (1988) *Quantum Many-Particle Physics* (Addison-Wesley, Reading)
- [32] Wilson K G and Kogut J (1974) *Phys. Rep.* **12** 75
- [33] Krishna-murthy H R, Wilkins J W and Wilson K G (1980) *Phys. Rev. B* **21** 1044
- [34] Costi T A, Hewson A C and Zlatić V (1994) *J. Phys. Cond. Matter* **6** 2519
- [35] Bulla R, Hewson A C and Pruschke Th (1998) *J. Phys. Cond. Matter* **10** 8365
- [36] Bulla R, Costi T A and Vollhardt D (2001) *Phys. Rev. B* **64** 45103
- [37] Hofstadter W (2000) *Phys. Rev. Lett.* **85** 1508
- [38] Verstraete F, Weichselbaum A, Schollwöck U, Cirac J I and von Delft J (2005) cond-mat/0504305
- [39] Anders F B and Schiller A (2005) *Phys. Rev. Lett.* **95** 196801
- [40] Pines D and Nozières (1966) *The Theory of Quantum Liquids, Vol I*. Benjamin W A, Inc. New York